Geophysical Research Letters

RESEARCH LETTER
10.1029/2022GL098539

Fine-Scale Geothermal Heat Flow in Antarctica Can Increase Simulated Subglacial Melt Estimates

Felicity S. McCormack[1], Jason L. Roberts[2], Christine F. Dow[3], Tobias Stål[4,5,6], Jacqueline A. Halpin[5,6], Anya M. Reading[4,5,6], and Martin J. Siegert[7]

[1]Securing Antarctica's Environmental Future, School of Earth, Atmosphere & Environment, Monash University, Clayton, VIC, Australia, [2]Australian Antarctic Division, Kingston, TAS, Australia, [3]Department of Geography and Environmental Management, University of Waterloo, Waterloo, ON, Canada, [4]School of Natural Sciences (Physics), University of Tasmania, Hobart, TAS, Australia, [5]Institute for Marine and Antarctica Studies, University of Tasmania, Hobart, TAS, Australia, [6]The Australian Centre for Excellence in Antarctic Science, University of Tasmania, Hobart, TAS, Australia, [7]Grantham Institute and Department of Earth Science and Engineering, Imperial College London, London, UK

Abstract Antarctic geothermal heat flow (GHF) affects the thermal regime of ice sheets and simulations of ice and subglacial meltwater discharge to the ocean, but remains poorly constrained. We use an ice sheet model to investigate the impact of GHF anomalies on subglacial meltwater production in the Aurora Subglacial Basin, East Antarctica. We find that spatially-variable GHF fields produce more meltwater than a constant GHF with the same background mean, and meltwater production increases as the resolution of GHF anomalies increases. Our results suggest that model simulations of this region systematically underestimate meltwater production using current GHF models. We determine the minimum basal heating required to bring the basal ice temperature to the pressure melting point, which should be taken together with the scale-length of likely local variability in targeting in-situ GHF field campaigns.

Plain Language Summary Geothermal heat flow (GHF) is important in controlling both the ice temperature and the production of meltwater at the base of the Antarctic Ice Sheet, which impacts how rapidly ice flows. However, GHF estimates are generally low resolution and highly uncertain. This uncertainty in GHF impacts the reliability of model simulations of the flow of ice and meltwater into the ocean, which in turn impacts estimates of the contribution of ice sheets to future sea level rise. We use an ice sheet model to investigate how spatial variations in GHF impact meltwater production in the Aurora Subglacial Basin (ASB), East Antarctica. GHF fields with spatial variations lead to consistently higher melt rates at the ice sheet base than a constant GHF field with the same mean value. We determine the minimum heat at the ice sheet base in the ASB required to cause the ice to melt, and highlight regions where small variations in GHF will have greater impacts on ice melting. These results show where measurements to constrain GHF should be prioritized to improve ice sheet model simulations.

Key Points:

- We present simulations of subglacial melt in the Aurora Subglacial Basin using various geothermal heat flow (GHF) fields
- Spatially-variable GHF enhances simulated subglacial melt compared with constant GHF
- We highlight where GHF measurements should be prioritized for improved estimates of subglacial melt

Supporting Information:

Supporting Information may be found in the online version of this article.

Correspondence to:

F. S. McCormack,
felicity.mccormack@monash.edu

Citation:

McCormack, F. S., Roberts, J. L., Dow, C. F., Stål, T., Halpin, J. A., Reading, A. M., & Siegert, M. J. (2022). Fine-scale geothermal heat flow in Antarctica can increase simulated subglacial melt estimates. *Geophysical Research Letters*, *49*, e2022GL098539. https://doi.org/10.1029/2022GL098539

Received 8 MAR 2022
Accepted 29 JUL 2022

Author Contributions:

Conceptualization: Felicity S. McCormack, Jason L. Roberts
Data curation: Felicity S. McCormack
Formal analysis: Felicity S. McCormack
Funding acquisition: Felicity S. McCormack
Investigation: Felicity S. McCormack
Methodology: Felicity S. McCormack, Jason L. Roberts
Project Administration: Felicity S. McCormack
Software: Felicity S. McCormack
Validation: Felicity S. McCormack
Visualization: Felicity S. McCormack
Writing – original draft: Felicity S. McCormack

1. Introduction

The timing of rapid glacier retreat and ice mass loss from key outlet basins in Antarctica constitutes the greatest uncertainty in estimates of future sea level rise (IPCC, 2021). The Aurora Subglacial Basin (ASB), East Antarctica, has significant potential to contribute to sea level rise (Pelle et al., 2020), containing approximately 7 m of sea-level equivalent ice (Morlighem et al., 2020), of which 3.5 m is grounded below sea level (Greenbaum et al., 2015). The ASB has dominated recent ice mass loss from East Antarctica, losing 20 ± 14 Gt year^{-1} of ice between 2003 and 2019 (Smith et al., 2020). While this loss is largely driven by ocean-induced melting of the Totten Ice Shelf (Adusumilli et al., 2020; Greene et al., 2017; Rintoul et al., 2016; Silvano et al., 2017), subglacial conditions that control ice flux to the margin, and thus the ocean, remain poorly understood.

Geophysical data reveal that the ASB has an active subglacial hydrological system (Wright et al., 2012), with an estimated annual discharge of approximately 1.3 Gt year^{-1} of water into the Totten cavity (Dow et al., 2020), representing 15% of the ice mass loss from this region. As in other regions of Antarctica and Greenland (Karlsson et al., 2021; Larour, Morlighem, et al., 2012; Siegert & Dowdeswell, 1996), for faster-flowing areas the primary heat source contributing to meltwater production in the ASB is likely to be frictional heating, with secondary contributions from GHF and other basal heat sources (Vieli et al., 2018). However, uncertainties in GHF in Antarctica and Greenland have been shown to compound uncertainties in ice and subglacial meltwater discharge

Writing – review & editing: Felicity S. McCormack, Jason L. Roberts, Christine F. Dow, Tobias Stål, Jacqueline A. Halpin, Anya M. Reading, Martin J. Siegert

estimates (Pittard, Galton-Fenzi et al., 2016; Pittard, Roberts, et al., 2016; Smith-Johnsen et al., 2020), demonstrating the need for improved constraints on this important, but often neglected, boundary condition.

A key source of uncertainty in Antarctic GHF is its spatial heterogeneity, particularly that associated with crustal processes and composition (Burton-Johnson et al., 2020), for which there are few constraints in the ice-covered interior. High spatial variability in GHF is likely in regions of southern Australia (McLaren et al., 2003; Pollett et al., 2019) that share geological affinities with the ASB (Maritati et al., 2019; Mulder et al., 2019; Stål et al., 2020). This relationship suggests that although the ASB has relatively stable tectonics, substantial spatial variability in GHF in this region is plausible, even likely. A recent model of Antarctic GHF (Stål et al., 2020) resolves variability down to 20 km resolution, albeit with large uncertainty. This is the highest resolution GHF model currently available for Antarctica, with most previous GHF models resolving variability to approximately 100 km resolution or lower. This means that the effect of any variability in GHF at scales <100 km has not typically been captured in ice sheet modeling studies, including in models used to predict the rate at which the Antarctic Ice Sheet will contribute to global sea level rise. Indeed, the impact of spatial variability in GHF at varying length scales on simulated basal ice temperature, and the consequent production of subglacial meltwater, remain largely unquantified in Antarctic ice sheet modeling applications. This has important implications for studies considering spatial heterogeneities in GHF, particularly due to the lack of guidance on what GHF length scales need to be resolved for ice sheet models and where efforts for further measurements to constrain GHF should be focused.

This study investigates the impact of hypothetical GHF anomalies, smoothed at varying length scales, on the simulation of where and how much subglacial meltwater is produced in the ASB using the Ice-sheet and Sea-level System Model (ISSM; Larour, Seroussi, et al., 2012). We determine where the ice sheet may be most sensitive to fine-scale, elevated GHF, which can be used to guide where future data collection should be prioritized to better resolve ice sheet dynamics.

2. Methods

2.1. Simulated GHF Fields

To investigate the impact of hypothetical GHF anomalies on subglacial meltwater production, we generate a 50-member ensemble of idealized, spatially-variable GHF fields covering the ASB. We assume that the GHF anomalies follow a Gaussian distribution:

$$G(x, y) = A \exp \frac{-\left[(x - x_i)^2 + (y - y_j)^2\right]}{2\sigma^2}, \quad (1)$$

with amplitude A, the radial scale of the anomaly σ, and center points (x_i, y_j). Here, the amplitude and standard deviation are generated using a Pearson system random number generation, where the statistics (mean, standard deviation, skewness, and kurtosis) are derived from modeled GHF anomalies along a transect in Prydz Bay, East Antarctica (Table S1 in Supporting Information S1, Carson et al., 2014). The center points (x_i, y_j) in Equation 1 are determined using a uniformly distributed random number generator. We assume that the ASB GHF anomalies occur at the same frequency as the Prydz Bay anomalies, that is, every 640 km^2, on average, which results in a total of 1,749 hotspots in the ASB for each ensemble member.

We calculate the area average of each randomly-sampled GHF anomaly field and adjust the background mean such that the overall area-averaged GHF in the ASB is 55 mW m^{-2}. The ensemble mean and the two ensemble end-members, with their corresponding subglacial melt rates, are shown in Figure S1 in Supporting Information S1. We apply a lowpass Gaussian filter to each field using filter cutoff lengths of 20, 40, 60, 80, 100, 200, 300, 400, and 500 km, where the response value of the filter at each cutoff length equals $\exp^{(-0.5)}$. This generates a total of 500 idealized GHF anomaly fields of varying smoothness.

2.2. Model Setup and Initialization

The horizontal mesh for the ice sheet model simulations comprises 1,553,265 anisotropic, prismatic elements, ranging from a refined mesh of 1 km resolution along the grounding line to a maximum of 4 km in the interior of the basin, and distributed over 10 vertical layers. The optimal mesh resolution was determined through sensitivity

analysis, the results of which are reported in Text S1 in Supporting Information S1. The catchment in-flow boundary velocities are constrained using observed ice surface velocities (Rignot et al., 2011, 2017), and the ice sheet geometry (ice surface elevation, thickness, bed) and grounding line are derived from BedMachine Antarctica (Morlighem et al., 2020). Surface temperatures are from RACMO2.3 (Lenaerts et al., 2012).

We use the Budd friction law (Budd et al., 1979) to apply friction at the base of the grounded ice sheet, and inverse methods (Morlighem et al., 2013) to calculate a spatially-varying basal friction coefficient. The inversion minimizes the misfit between the observed and simulated surface velocities, using logarithmic and linear misfits as well as Tikhonov regularization. The basal friction coefficient is shown in Figure S2a in Supporting Information S1. The area-weighted median percentage difference between the modeled and observed surface velocities for the entire catchment is −9.4%. We use a Glen flow relation (Glen, 1952, 1953, 1955) with a stress exponent of $n = 3$, where the ice rigidity B is calculated using inverse methods (Figure S2b in Supporting Information S1).

2.3. Model Experiments

We perform an ensemble of simulations using each of the 500 GHF anomaly fields and a control case where the GHF is a spatially constant 55 mW m^{-2}. For the control case, we use the output of a diffusion-only 3-dimensional thermal model to specify temperatures at the catchment boundaries (step 1). We then perform a diagnostic simulation using the Blatter-Pattyn (Blatter, 1995; Pattyn, 2003) approximation to the full Stokes equations (step 2) to determine steady-state velocities, using these to then calculate steady-state englacial temperatures through simulation of an enthalpy formulation (Aschwanden et al., 2012) of the thermal model implemented in ISSM (Seroussi et al., 2013) (step 3). For each of the GHF anomaly fields, we perform steps 1 and 3, using the same velocity field as the constant GHF case.

2.4. Calculating the Minimum Heating for Subglacial Melt

We calculate the minimum basal heat flow from secondary sources (i.e., excluding frictional heating) required to bring the basal temperature to pressure melting point, $Q_{S_{\min}}$, using the following iterative method. We start by calculating a steady-state temperature (steps 1 and 3 from Section 2.3) using a uniform GHF field of zero mW m^{-2} across the ASB. From this output, we identify regions where the basal temperature is at the pressure melting point due to frictional heating alone, and exclude these regions and the ice shelf from the adjustment procedure that follows. Elsewhere across the catchment, we uniformly increase the basal heat flow (nominally the model GHF field) by $c = 0.1$ mW m^{-2} and repeat step 3. The element-wise adjusted basal heat flow (BHF) for the next iteration is then

$$BHF_i = BHF_{i-1} + \delta_i c, \tag{2}$$

where i is the current iteration. The term $\delta_0 = 1$ and δ_i is defined as follows:

$$\delta_i = \begin{cases} \delta_{i-1}, & \text{if } T_{b_i} - T_{pmp} < -\varepsilon \text{ and } T_{b_{i-1}} - T_{pmp} < -\varepsilon \\ \frac{1}{2}\delta_{i-1}, & \text{if } T_{b_i} - T_{pmp} \geq \varepsilon \text{ and } T_{b_{i-1}} - T_{pmp} \geq \varepsilon \\ -\frac{1}{2}\delta_{i-1}, & \text{if } T_{b_i} - T_{pmp} \geq \varepsilon \text{ and } T_{b_{i-1}} - T_{pmp} < -\varepsilon \\ -\frac{1}{2}\delta_{i-1}, & \text{if } T_{b_i} - T_{pmp} < -\varepsilon \text{ and } T_{b_{i-1}} - T_{pmp} \geq \varepsilon \\ 0, & \text{otherwise} \end{cases} \tag{3}$$

Here, T_{b_i} is the basal temperature at iteration i, T_{pmp} is the basal temperature at the pressure melting point, and $\varepsilon = 10^{-5}$°C. We iterate through these steps, incrementally changing the BHF at each mesh vertex, until either the simulated basal temperature at that vertex is within 10^{-5}°C of pressure melting point, or the BHF at that vertex exceeds an arbitrary threshold of 160 mW m^{-2}.

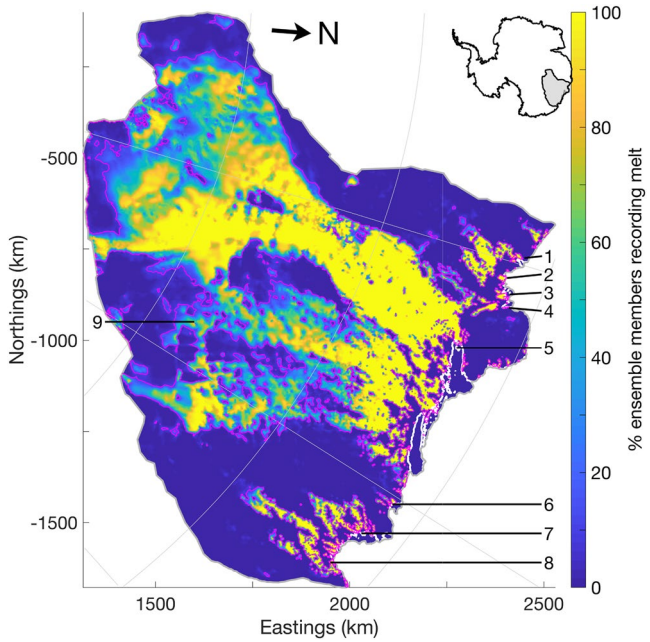

Figure 1. Percentage of the 500 ensemble members in which melt is recorded. Eastings and northings are for a polar stereographic projection with 71°S the latitude of true scale and 0°E the reference meridian. The magenta contour outlines where 10% of members predict melt to occur. The light gray contour shows the Aurora Subglacial Basin (ASB) domain; the white contour shows the ice-ocean front and grounding line. Key outlet glaciers of the ASB are indicated as follows: Underwood Glacier (1), Bond Glacier (2), Adams Glacier (3), Vanderford Glacier (4), Totten Glacier (5), Blair Glacier (6), Holmes Glacier (7), and Frost Glacier (8). Highland C in the interior of the catchment is also indicated (9). There is strong agreement between the ensemble members in the region where melt occurs.

3. Results

3.1. Subglacial Meltwater Production

The locations where the basal temperatures are at the pressure melting point and where meltwater is likely to be produced are consistent across ensemble members (Figure 1). In most ensemble members, meltwater is concentrated in the tributaries that feed key ASB outlet glaciers. A smaller proportion of ensemble members predict meltwater in the sedimentary interior of the ASB, south of Highland C (Aitken et al., 2016), where ice is thickest. For large swaths of the catchment there is almost no meltwater production among the 500 ensemble members, even with a uniform distribution of GHF hotspots (Figure S1a–S1f in Supporting Information S1). This indicates that certain locations are highly sensitive to the presence of GHF hotspots for meltwater production, while others remain insensitive.

We next calculate the area-averaged melt rate in regions of the ASB where at least 10% of the ensemble members predict melt to occur (Figure 1). In the spatially-constant GHF field, this produces an area-averaged melt rate (M_c) of 3.97 mm year^{-1} (Figure 2a). However, each of the 500 spatially-varying ensemble members predict higher area-averaged melt rates (M_E) than the constant GHF case in these regions, with a maximum increase of 4.53%.

A consistent trend emerges in the impact of the smoothness of the variable GHF fields on the area-averaged melt rates across the ASB (Figure 2b). Melt rates generally decrease with increasing lowpass filter cutoff length, reaching a minimum for GHF fields that are lowpass filtered on the 100–200 km scale, and increasing for greater filter cutoff lengths. This is because as GHF maxima are smoothed and reduced, the background GHF increases. However, the increase in the background GHF, and consequent increase in the total area where the background basal temperature is at the pressure melting point, is not sufficient to offset decreased melting over GHF hotspots,

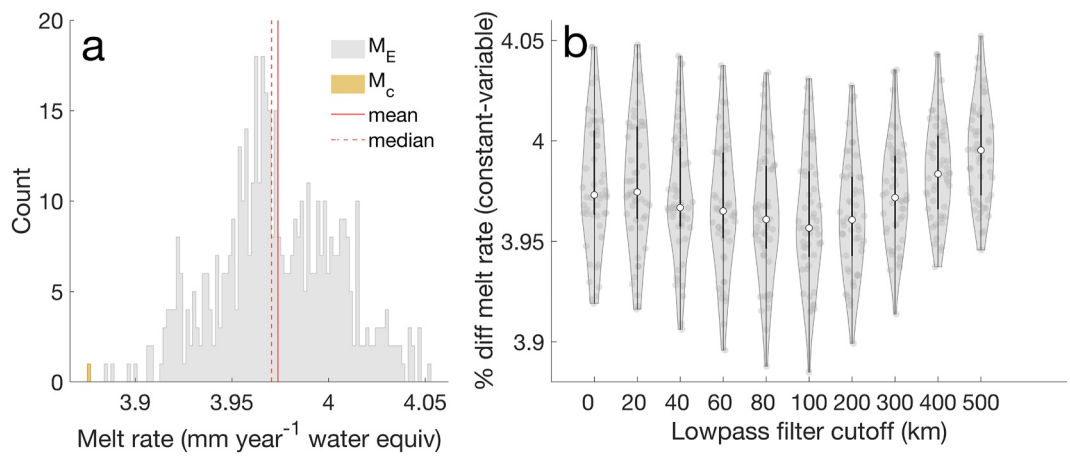

Figure 2. Modeled subglacial melt rates (mm year^{-1}, water equivalent). (a) Distribution of subglacial melt rates for the spatially-variable geothermal heat flow (GHF) ensemble members (M_E; gray) and for the constant GHF field (M_c; orange), averaged over the region where at least 10% of ensemble members predict melt to occur. The mean and median melt rates for the ensemble are shown in solid and dashed red lines, respectively. (b) Violin plot of the percentage difference between the melt rates of the spatially-variable GHF ensemble members and that of the constant GHF field, for each lowpass filtered data set. The median value is shown as a circle; the bold black line shows the 25th–75th percentiles; the violin extends to the most extreme data points; light gray circles show each ensemble member; and the area of the violin is the kernel density estimate of the data. The spatially-variable GHF members consistently yield higher melt rates than the spatially-constant GHF field, and melt rates are minimized for filter cutoff lengths of 100 km.

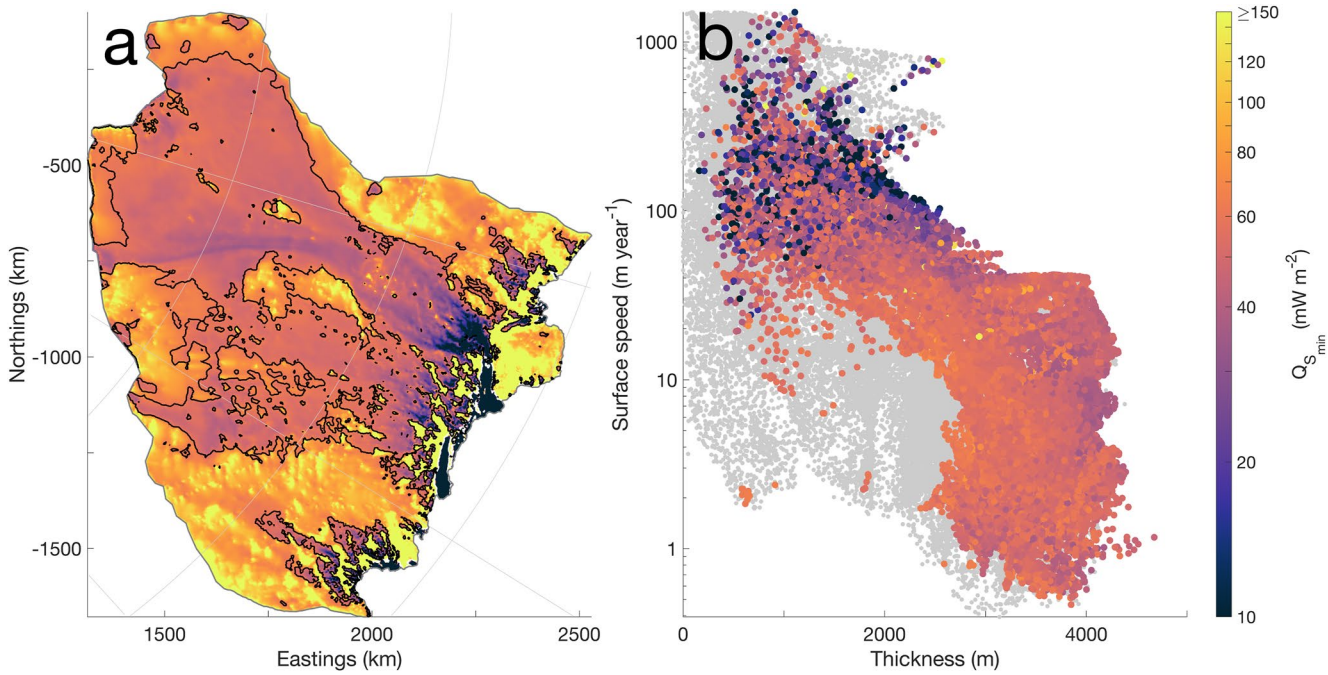

Figure 3. Spatial distribution of $Q_{S_{min}}$ and its relationship with ice thickness and surface speed. (a) Minimum heat required to bring basal temperatures to pressure melting point ($Q_{S_{min}}$; mW m^{-2}). The black contour outlines where 10% of members predict melt to occur. The light gray and white contours are the same as in Figure 1. (b) Thickness (m) versus surface speed (m year^{-1}). The colored points are values of $Q_{S_{min}}$ (mW m^{-2}) recorded in model grid cells where at least 10% of ensemble members predict melt to occur. The gray points represent cells where fewer than 10% of the ensemble members predict melt to occur. Logarithmic axes for $Q_{S_{min}}$ are used in both panels, and a logarithmic axis for surface speeds is used in panel (b).

except for filter cutoff lengths over approximately 200 km. We find that the ensemble mean for the 100 km filter cutoff length is statistically significantly ($p < 0.05$) different to the unfiltered GHF field using a two-sample *t*-test (Table S2 in Supporting Information S1). Given that many of the currently-available GHF estimates used in ice sheet modeling applications are approximately 100–200 km resolution (An et al., 2015; Martos et al., 2017; Maule et al., 2005; Shapiro & Ritzwoller, 2004; Shen et al., 2020), this implies that subglacial melt rates have been systematically underestimated when using such GHF models.

3.2. Minimum Basal Heat Required to Produce Meltwater

We examine the minimum basal heat from secondary sources ($Q_{S_{min}}$; i.e., excluding frictional heating) that is required to bring the basal temperature to the pressure melting point, given simulated ice velocity and thickness fields representative of present-day (Section 2.4). $Q_{S_{min}}$ (Figure 3a) is lower in regions where a large proportion of ensemble members predict melt; the area-averaged $Q_{S_{min}}$ is 50 ± 12 mW m^{-2} in regions where at least 10% of the ensemble members predict melt to occur, less than the basin average value of 55 mW m^{-2}. Meltwater production in these regions is likely to be particularly sensitive to fine-scale and elevated GHF. Outside these regions, the area-averaged $Q_{S_{min}}$ is 96 ± 33 mW m^{-2}; in some regions, a value of $Q_{S_{min}} = 160$ mW m^{-2} is insufficient to produce meltwater.

To understand the physical processes and underlying environmental conditions that lead to meltwater production, we investigate the relationship between $Q_{S_{min}}$ and the corresponding ice thickness and ice surface speed (Figure 3b). Again considering the regions where at least 10% of the ensemble members predict melt to occur, some broad patterns emerge. For regions of streaming flow (where surface speeds exceed 50 m year^{-1}) where the ice is generally less than 2,500 m thick, $Q_{S_{min}} = 38 \pm 15$ mW m^{-2} and is approximately uniformly distributed (Figure S3a in Supporting Information S1). Outside regions of streaming flow, $Q_{S_{min}}$ continues to show strong dependence on ice flow, increasing for decreasing surface speed between ice thicknesses of 2,000 and 3,300 m (Figures S3b and S3bc in Supporting Information S1). For ice thicker than 3,300 m, $Q_{S_{min}}$ decreases with increasing thickness, irrespective of surface speed.

Sources that contribute to $Q_{S_{\min}}$ include GHF, deformational heating, and latent heating associated with subglacial meltwater transport. The deformational heating at the base Q_D can be estimated from:

$$Q_D = 4\mu\dot{\epsilon}_e^2, \tag{4}$$

where μ is the viscosity (Pas), and $\dot{\epsilon}_e$ is the effective strain rate (s^{-1}), the second invariant of the strain rate tensor, given by $\dot{\epsilon}_e = \sqrt{\mathrm{tr}\,(\dot{\epsilon}^2)/2}$. We compare $Q_{S_{\min}}$ and Q_D in Figure S5 in Supporting Information S1. Deformational heating increases toward the ice margin, where it is a dominant contributor to basal heating. Elsewhere in the catchment Q_D is much lower than $Q_{S_{\min}}$. This includes large parts of the main Totten tributary and where at least 10% of the ensemble members predict melt to occur, reinforcing the importance of GHF in these regions.

Previous work (Pattyn, 2010) used a simplification of analytic methods (Hindmarsh, 1999) to derive $Q_{S_{\min}}$ for the Antarctic Ice Sheet, finding that meltwater is generally present for $Q_{S_{\min}}$ ~40 mW m^{-2}. Although we find that $Q_{S_{\min}}$ is substantially lower than 40 mW m^{-2} in some regions of streaming flow, our spatial patterns in $Q_{S_{\min}}$ in the ASB show similarities to those in Pattyn (2010). Our results also reveal nuances in the dependence of $Q_{S_{\min}}$ on the underlying environmental conditions—the ice thickness and surface speeds. Our model suggests that ice speed is an important controlling factor in the $Q_{S_{\min}}$ value, and that a critical thickness of 3,300 m must be reached before ice thickness effects lead to reductions in $Q_{S_{\min}}$. Ice speed may be a more important diagnostic than ice thickness in predicting $Q_{S_{\min}}$ in some regions, with the effect of very slow flow sometimes weighing more strongly in the determination of a very high $Q_{S_{\min}}$ than the effect of thick ice (e.g., the region south east of Highland C Figure 3a).

4. Discussion

In regions of Earth's surface where GHF can be readily derived from in-situ measurements, substantial spatial variability in this field is commonly observed (Goutorbe et al., 2011; McLaren et al., 2003; Rolandone et al., 2002). Assuming that this is also the case in the ASB, we investigate the impact of hypothetical spatial variability in GHF, of varying smoothness, on subglacial meltwater production. We find higher subglacial melt rates for all cases of spatially-variable GHF fields.

We also find that the simulated meltwater estimates are lowest for GHF fields smoothed using a ~100 km lowpass filter length cutoff, and increases for both less smooth and smoother GHF fields. This indicates that the GHF fields most widely used in ice sheet modeling applications—typically representing anomalies at the 100 km scale—likely systematically underestimate basal meltwater production. Our results indicate that the inclusion of fine-scale GHF anomalies, for example, at resolutions of 20 km or finer, are important for more robust simulations of: (a) where the ice sheet is flowing by sliding; and (b) the relative contributions of meltwater and ice mass to the ice sheet mass loss budget (e.g., Karlsson et al., 2021).

Given our results for the impact of fine-scale GHF on subglacial meltwater production, and the difficulty in accurately constraining GHF heterogeneities (e.g., associated with crustal heat production), the next question is where and how to prioritize measurements to constrain GHF and models that robustly incorporate fine-scale GHF? We present a novel method for determining the minimum heat flow from secondary sources required to bring the basal temperatures to the pressure melting point $\left(Q_{S_{\min}}\right)$ and how it varies across the ASB. We link this heat flow to the underlying physical and environmental characteristics of the ASB. The $Q_{S_{\min}}$ field highlights regions of the ASB that may be particularly sensitive to fine-scale or elevated GHF, that is, in the main tributaries feeding the key outlet glaciers of the ASB, regions of streaming flow (where the ice surface speeds exceed 50 m $year^{-1}$), and in the deep interior of the basin. Based on our $Q_{S_{\min}}$ field, we delineate regions of the ASB into different priority zones: (a) regions in the interior of the catchment where GHF is potentially a dominant heat source over frictional heating (defined where the surface speed is <300 m $year^{-1}$), but where the GHF uncertainty exceeds 20 mW m^{-2} (Stål et al., 2020), and where our modeling shows at least 10% of ensemble members predict a wet bed; (b) regions where at least 10% of ensemble members predict a wet bed, but where the ice surface speed >300 m $year^{-1}$ or the GHF uncertainty is <20 mW m^{-2}; and (c) regions where fewer than 10% of ensemble members predict a wet bed. These priority regions are highlighted in Figure 4 and can be used to guide efforts for collection of future measurements to constrain GHF in the ASB. For instance, Figure 4 suggests that borehole targets should be prioritized within the priority one zone, and that scale-length information, including from airborne geophysics or predictions from likely geology, must also be obtained within this region to provide

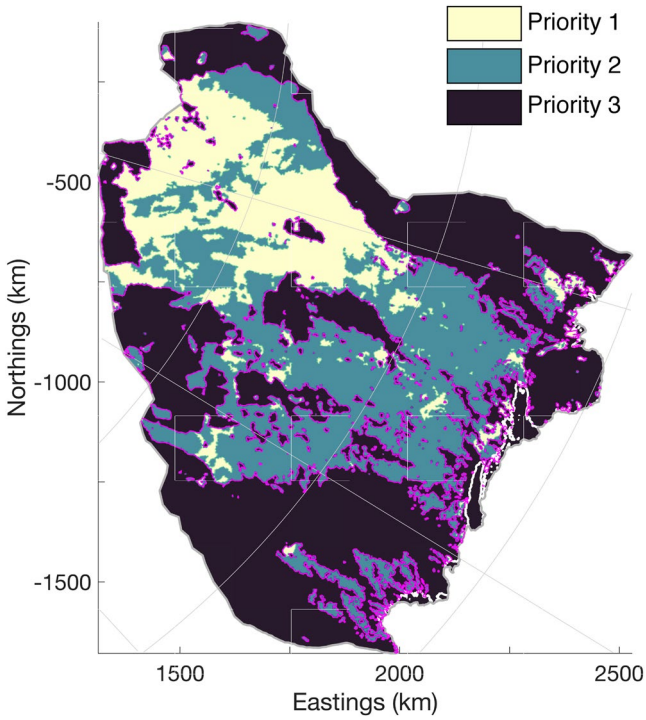

Figure 4. Priority zones for in-situ geothermal heat flow (GHF) field campaigns, including from boreholes and using geophysics. Priority 1 zones (yellow) are defined where at least 10% of ensemble members predict subglacial meltwater production, the ice surface speed is <300 m year^{-1}, and there is relatively high uncertainty in GHF estimates (Stål et al., 2020); priority 2 zones (green) are defined elsewhere where at least 10% of ensemble members predict subglacial meltwater production; and priority 3 zones (dark blue) are defined where fewer than 10% of ensemble members predict subglacial meltwater production. The magenta, light gray, and white contours are the same as in Figure 1.

a context to GHF estimates from borehole measurements. Our modeling of $Q_{S_{\min}}$ can be extended to other regions in Antarctica to narrow the target zone for measurements. This approach can also be used to guide novel analyses of existing datasets that aid in constraining GHF, for example, assimilation of radar- or seismic-derived estimates of englacial temperatures, subglacial water distribution or englacial layer dating and satellite evidence of englacial lakes. These constraints may further aid efforts to estimate subglacial meltwater production and ice flow by sliding and internal deformation and have benefit in reducing uncertainties associated with other model parameters, for example, the basal friction coefficient, and in future efforts toward improved modeling of the subglacial environment.

The spatially-variable GHF fields generated in this study are idealized and are not an attempt to represent the actual spatial heterogeneity in crustal heat flow in the ASB, although Antarctic GHF is unlikely to be spatially constant and knowledge of its fine-scale structure is limited. Future work should explore the effect of different realizations of spatial variability in GHF—including variability that depends on the underlying geology (Burton-Johnson et al., 2020; Seroussi et al., 2017)—on the dynamics of, interactions between, and variability in the ice sheet and subglacial hydrology systems.

Finally, our analysis estimates, for present conditions, the impact of variable GHF on local subglacial meltwater production and does not take into account the dynamical nature of the subglacial hydrological system or the ice sheet system and their interactions. Accounting for the transport of meltwater through coupling between the ice sheet and its subglacial hydrological system may redistribute basal heat (Vieli et al., 2018) and meltwater production. If fine-scale GHF is incorporated, and the magnitude of meltwater production subsequently increases as we have shown, this could lead to an increase in estimates of subglacial meltwater discharge across the grounding zone and into any ice shelf cavities. It could also lead to an acceleration in ice flow extending hundreds of kilometers from the perturbation, as has been previously demonstrated (Pittard, Galton-Fenzi et al., 2016; Pittard, Roberts, et al., 2016; Smith-Johnsen et al., 2020). Furthermore, the location of GHF hotspots, and hence the locations of increased meltwater production, will impact the dynamics of the subglacial hydrological network, including where subglacial channels can form, and where and how much meltwater volume will be directed into any ice shelf cavities. For example, increased meltwater production in the deep interior of the catchment will impact local sliding rates; however, this increase in meltwater may have little effect on channels near the grounding line due to the inefficiency of the interior distributed hydrological systems in routing subglacial meltwater (Dow et al., 2020). By contrast, increased water production in the troughs feeding subglacial channels and in the regions of fast-flowing ice may have a significant impact on ice dynamics through the increased efficiency of channelized systems. These are important considerations that warrant further investigation.

5. Conclusions

In this study we explore the impact of idealized, spatially-variable GHF fields on simulated subglacial meltwater production in the Aurora Subglacial Basin. We find that spatially-variable GHF fields produce more meltwater than a constant GHF with the same background mean, and that subglacial meltwater estimates increase as the resolution of GHF anomalies increases. Our results indicate subglacial meltwater volume calculated from model simulations of this region are systematically underestimated. This may have implications for both biases and uncertainties associated with projections of ice flux into the ocean and the magnitude of subglacial meltwater discharge into ice shelf cavities. We recommend the inclusion of fine-scale GHF anomalies in ice sheet modeling applications, for example, at resolutions of 20 km or finer, to constrain: (a) subglacial meltwater estimates, including the relative contributions of meltwater and ice mass to the ice sheet mass loss budget; and (b) where

the ice sheet is flowing by sliding or internal deformation. We calculate the minimum basal heat flow required to bring the basal ice temperature to the pressure melting point, and delineate priority regions within the Aurora Subglacial Basin where efforts could be focused to constrain the magnitude and variability in GHF, including from borehole measurements as well as scale-length information from geophysics or geology. Our analysis highlights the need for ensemble simulations of ice sheet models that include spatially-variable GHF fields, and the development of coupled ice sheet-subglacial hydrology models to account for feedbacks between ice sheet thermo-mechanics and subglacial meltwater production, distribution, and discharge.

Data Availability Statement

The data and source code used in this study are publicly available. We use version 4.19 of the open source ISSM software, which is available for download from https://issm.jpl.nasa.gov/download/. The model initialization datasets are publicly available and found in the relevant citations, specifically: surface velocities (Rignot et al., 2011, 2017); ice surface elevation, thickness, bed and grounding line data (Morlighem et al., 2020); and surface temperatures (Lenaerts et al., 2012).

Acknowledgments
The authors thank two anonymous reviewers for their constructive feedback. FSM was supported under an Australian Research Council (ARC) Discovery Early Career Research Award (DE210101433) and the ARC Special Research Initiative Securing Antarctica's Environmental Future (SR200100005). This research was undertaken with the assistance of resources from the National Computational Infrastructure, which is supported by the Australian Government. TS and AMR were supported by ARC Discovery Project (DP190100418) and the ARC Special Research Initiative, Australian Centre for Excellence in Antarctic Science (ACEAS, SR200100008). JH was supported by ACEAS (SR200100008) and ARC Discovery Project (DP180104074). CD was supported by the Canada Research Chairs Program (950-231237).

References

Adusumilli, S., Fricker, H. A., Medley, B., Padman, L., & Siegfried, M. R. (2020). Interannual variations in meltwater input to the Southern Ocean from Antarctic ice shelves. *Nature Geoscience*, *13*(9), 616–620. https://doi.org/10.1038/s41561-020-0616-z

Aitken, A. R. A., Roberts, J. L., van Ommen, T. D., Young, D. A., Golledge, N. R., Greenbaum, J. S., et al. (2016). Repeated large-scale retreat and advance of Totten Glacier indicated by inland bed erosion. *Nature*, *533*(7603), 385–389. https://doi.org/10.1038/nature17447

An, M., Wiens, D. A., Zhao, Y., Feng, M., Nyblade, A., Kanao, M., et al. (2015). Temperature, lithosphere-asthenosphere boundary, and heat flux beneath the Antarctic Plate inferred from seismic velocities. *Journal of Geophysical Research: Solid Earth*, *120*(12), 8720–8742. https://doi.org/10.1002/2015JB011917

Aschwanden, A., Bueler, E., Khroulev, C., & Blatter, H. (2012). An enthalpy formulation for glaciers and ice sheets. *Journal of Glaciology*, *58*(209), 441–457. https://doi.org/10.3189/2012JoG11J088

Blatter, H. (1995). Velocity and stress-fields in grounded glaciers: A simple algorithm for including deviatoric stress gradients. *Journal of Glaciology*, *41*(138), 333–344. https://doi.org/10.3189/S002214300001621X

Budd, W. F., Keage, P. L., & Blundy, N. A. (1979). Empirical studies of ice sliding. *Journal of Glaciology*, *23*(89), 157–170. https://doi.org/10.3189/S0022143000029804

Burton-Johnson, A., Dziadek, R., & Martin, C. (2020). Review article: Geothermal heat flow in Antarctica: Current and future directions. *The Cryosphere*, *14*(11), 3843–3873. https://doi.org/10.5194/tc-14-3843-2020

Carson, C. J., McLaren, S., Roberts, J. L., Boger, S. D., & Blankenship, D. D. (2014). Hot rocks in a cold place: High sub-glacial heat flow in East Antarctica. *Journal of the Geological Society*, *171*, 9–12. https://doi.org/10.1144/jgs2013-030

Dow, C. F., McCormack, F. S., Young, D. A., Greenbaum, J. S., Roberts, J. L., & Blankenship, D. D. (2020). Totten Glacier subglacial hydrology determined from geophysics and modeling. *Earth and Planetary Science Letters*, *531*, 115961. https://doi.org/10.1016/j.epsl.2019.115961

Glen, J. W. (1952). Experiments on the deformation of ice. *Journal of Glaciology*, *2*(12), 111–114. https://doi.org/10.3189/S0022143000034067

Glen, J. W. (1953). Rate of flow of polycrystalline ice. *Nature*, *172*(4381), 721–722. https://doi.org/10.1038/172721a0

Glen, J. W. (1955). The creep of polycrystalline ice. *Proceedings of the Royal Society A*, *228*(1175), 519–538. https://doi.org/10.1098/rspa.1955.0066

Goutorbe, B., Poort, J., Lucazeau, F., & Raillard, S. (2011). Global heat flow trends resolved from multiple geological and geophysical proxies. *Geophysical Journal International*, *187*(3), 1405–1419. https://doi.org/10.1111/j.1365-246X.2011.05228.x

Greenbaum, J. S., Blankenship, D. D., Young, D. A., Richter, T. G., Roberts, J. L., Aitken, A. R. A., et al. (2015). Ocean access to a cavity beneath Totten Glacier in East Antarctica. *Nature Geoscience*, *8*(4), 294–298. https://doi.org/10.1038/ngeo2388

Greene, C. A., Blankenship, D. D., Gwyther, D. E., Silvano, A., & van Wijk, E. (2017). Wind causes Totten Ice Shelf melt and acceleration. *Science Advances*, *3*(11), e1701681. https://doi.org/10.1126/sciadv.1701681

Hindmarsh, R. (1999). On the numerical computation of temperature in an ice sheet. *Journal of Glaciology*, *45*(151), 568–574. https://doi.org/10.1017/9781009157896

IPCC. (2021). *Climate change 2021: The physical science Basis. Contribution of Working Group I to the Sixth Assessment Report of the Intergovernmental Panel on Climate Change*. In V. Masson-Delmotte, P. Zhai, H.-O. Pörtner, D. Roberts, J. Skea, et al. (Eds.), Cambridge University Press. https://doi.org/10.1017/9781009157896

Karlsson, N. B., Solgaard, A. M., Mankoff, K. D., Gillet-Chaulet, F., MacGregor, J. A., Box, J. E., et al. (2021). A first constraint on basal melt-water production of the Greenland Ice Sheet. *Nature Communications*, *12*(3461). https://doi.org/10.1038/s41467-021-23739-z

Larour, E., Morlighem, M., Seroussi, H., Schiermeier, J., & Rignot, E. (2012). Ice flow sensitivity to geothermal heat flux of Pine Island Glacier, Antarctica. *Journal of Geophysical Research*, *117*, F04023. https://doi.org/10.1029/2012JF002371

Larour, E., Seroussi, H., Morlighem, M., & Rignot, E. (2012). Continental scale, high order, high spatial resolution, ice sheet modeling using the Ice Sheet System Model (ISSM). *Journal of Geophysical Research*, *117*(F01022), 1–20. https://doi.org/10.1029/2011JF002140

Lenaerts, J. T. M., van den Broeke, M. R., van de Berg, W. J., van Meijgaard, E., & Munneke, P. K. (2012). A new, high-resolution surface mass balance map of Antarctica (1979–2010) based on regional atmospheric climate modeling. *Geophysical Research Letters*, *39*(4), 1–5. https://doi.org/10.1029/2011GL050713

Maritati, A., Halpin, J. A., Whittaker, J. M., & Daczko, N. R. (2019). Fingerprinting Proterozoic bedrock in interior Wilkes Land, East Antarctica. *Scientific Reports*, *9*(1), 10192. https://doi.org/10.1038/s41598-019-46612-y

Martos, Y. M., Catalán, M., Jordan, T. A., Golynsky, A., Golynsky, D., Eagles, G., & Vaughan, D. G. (2017). Heat flux distribution of Antarctica unveiled. *Geophysical Research Letters*, *44*(22), 11417–11426. https://doi.org/10.1002/2017GL075609

Maule, C. F., Purucker, M. E., Olsen, N., & Mosegaard, K. (2005). Heat flux anomalies in Antarctica revealed by Satellite magnetic data. *Science*, *309*(5733), 464–467. https://doi.org/10.1126/science.1106888

McLaren, S., Sandiford, M., Hand, M., Neumann, N., Wyborn, L., & Bastrakova, I. (2003). The hot southern continent: Heat flow and heat production in Australian Proterozoic terranes. *Special Paper of the Geological Society of America*, *372*, 157–167. https://doi.org/10.1130/0-8137-2372-8.157

Morlighem, M., Rignot, E., Binder, T., Blankenship, D., Drews, R., Eagles, G., et al. (2020). Deep glacial troughs and stabilizing ridges unveiled beneath the margins of the Antarctic Ice Sheet. *Nature Geoscience*, *13*(2), 132–137. https://doi.org/10.1038/s41561-019-0510-8

Morlighem, M., Seroussi, H., Larour, E., & Rignot, E. (2013). Inversion of basal friction in Antarctica using exact and incomplete adjoints of a higher-order model. *Journal of Geophysical Research*, *118*(3), 1746–1753. https://doi.org/10.1002/jgrf.20125

Mulder, J. A., Halpin, J. A., Daczko, N. R., Orth, K., Meffre, S., Thompson, J. M., & Morrissey, L. J. (2019). A multiproxy provenance approach to uncovering the assembly of East Gondwana in Antarctica. *Geology*, *47*(7), 645–649. https://doi.org/10.1130/G45952.1

Pattyn, F. (2003). A new three-dimensional higher-order thermomechanical ice sheet model: Basic sensitivity, ice stream development, and ice flow across subglacial lakes. *Journal of Geophysical Research*, *108*(B8), 1–15. https://doi.org/10.1029/2002JB002329

Pattyn, F. (2010). Antarctic subglacial conditions inferred from a hybrid ice sheet/ice stream model. *Earth and Planetary Science Letters*, *295*(3–4), 451–461. https://doi.org/10.1016/j.epsl.2010.04.025

Pelle, T., Morlighem, M., & McCormack, F. S. (2020). Aurora Basin, the weak underbelly of East Antarctica. *Geophysical Research Letters*, *47*(9), e2019GL086821. https://doi.org/10.1029/2019GL086821

Pittard, M. L., Galton-Fenzi, B. K., Roberts, J. L., & Watson, C. S. (2016). Organization of ice flow by localized regions of elevated geothermal heat flux. *Geophysical Research Letters*, *43*(7), 3342–3350. https://doi.org/10.1002/2016GL068436

Pittard, M. L., Roberts, J. L., Galton-Fenzi, B. K., & Watson, C. S. (2016). Sensitivity of the Lambert-Amery glacial system to geothermal heat flux. *Annals of Glaciology*, *57*(73), 56–68. https://doi.org/10.1017/aog.2016.26

Pollett, A., Hasterok, D., Raimondo, T., Halpin, J. A., Hand, M., Bendall, B., & McLaren, S. (2019). Heat flow in southern Australia and connections with East Antarctica. *Geochemistry, Geophysics, Geosystems*, *20*(11), 5352–5370. https://doi.org/10.1029/2019GC008418

Rignot, E., Mouginot, J., & Scheuchl, B. (2011). Ice flow of the Antarctic Ice Sheet. *Science*, *333*(6048), 1427–1430. https://doi.org/10.1126/science.1208336

Rignot, E., Mouginot, J., & Scheuchl, B. (2017). MEaSUREs InSAR-based Antarctica ice velocity map 450 m Version 2.0. NASA National Snow and Ice Data Center Distributed Active Archive Center. https://doi.org/10.5067/D7GK8F5J8M8R

Rintoul, S. R., Silvano, A., Pena-Molino, B., van Wijk, E., Rosenberg, M., Greenbaum, J. S., & Blankenship, D. D. (2016). Ocean heat drives rapid basal melt of the Totten Ice Shelf. *Science Advances*, *2*(12), e1601610. https://doi.org/10.1126/sciadv.1601610

Rolandone, F., Jaupart, C., Mareschal, J. C., Gariépy, C., Bienfait, G., Carbonne, C., & Lapointe, R. (2002). Surface heat flow, crustal temperatures and mantle heat flow in the Proterozoic Trans-Hudson Orogen, Canadian Shield. *Journal of Geophysical Research*, *107*(B12), 2341. https://doi.org/10.1029/2001jb000698

Seroussi, H., Ivins, E. R., Wiens, D. A., & Bondzio, J. (2017). Influence of a West Antarctic mantle plume on ice sheet basal conditions. *Journal of Geophysical Research: Solid Earth*, *122*(9), 7127–7155. https://doi.org/10.1002/2017JB014423

Seroussi, H., Morlighem, M., Rignot, E., Khazendar, A., Larour, E., & Mouginot, J. (2013). Dependence of century-scale projections of the Greenland ice sheet on its thermal regime. *Journal of Glaciology*, *59*(218), 1024–1034. https://doi.org/10.3189/2013JoG13J054

Shapiro, N., & Ritzwoller, M. (2004). Inferring surface heat flux distributions guided by a global seismic model: Particular application to Antarctica. *Earth and Planetary Science Letters*, *223*(1–2), 213–224. https://doi.org/10.1016/j.epsl.2004.04.011

Shen, W., Wiens, D. A., Lloyd, A. J., & Nyblade, A. A. A. (2020). A geothermal heat flux map of Antarctica empirically constrained by seismic structure. *Geophysical Research Letters*, *47*(e2020GL086955). https://doi.org/10.1029/2020GL086955

Siegert, M. J., & Dowdeswell, J. A. (1996). Spatial variations in heat at the base of the Antarctic Ice Sheet from analysis of the thermal regime above subglacial lakes. *Journal of Glaciology*, *42*(142), 501–509. https://doi.org/10.3189/S0022143000003488

Silvano, A., Rintoul, S. R., Peña-Molino, B., & Williams, G. D. (2017). Distribution of water masses and meltwater on the continental shelf near the Totten and Moscow University ice shelves. *Journal of Geophysical Research: Oceans*, *122*(3), 2050–2068. https://doi.org/10.1002/2016JC012115

Smith, B., Fricker, H. A., Gardner, A. S., Medley, B., Nilsson, J., Paolo, F. S., et al. (2020). Pervasive ice sheet mass loss reflects competing ocean and atmosphere processes. *Science*, *368*(6496), 1239–1242. https://doi.org/10.1126/science.aaz5845

Smith-Johnsen, S., Schlegel, N.-J., De Fleurian, B., & Nisancioglu, K. H. (2020). Sensitivity of the Northeast Greenland Ice Stream to geothermal heat. *Journal of Geophysical Research: Earth Surface*, *125*(1), e2019JF005252. https://doi.org/10.1029/2019JF005252

Stål, T., Reading, A. M., Halpin, J. A., & Whittaker, J. M. (2020). Antarctic geothermal heat flow model: Aq1. *Geochemistry, Geophysics, Geosystems*, *22*(2), e2020GC009428. https://doi.org/10.1029/2020GC009428

Vieli, G.-M. L., Martin, C., Hindmarsh, R., & Lüthi, M. P. (2018). Basal freeze-on generates complex ice-sheet stratigraphy. *Nature Communications*, *9*(1), 4669. https://doi.org/10.1038/s41467-018-07083-3

Wright, A. P., Young, D. A., Roberts, J. L., Schroeder, D. M., Bamber, J. L., Dowdeswell, J. A., et al. (2012). Evidence of a hydrological connection between the ice divide and ice sheet margin in the Aurora Subglacial Basin, East Antarctica. *Journal of Geophysical Research*, *117*(F1), 010333–F1115. https://doi.org/10.1029/2011JF002066